IMMUNOLOGY

Microbiota-derived peptide mimics drive lethal inflammatory cardiomyopathy

Cristina Gil-Cruz[1], Christian Perez-Shibayama[1], Angelina De Martin[1], Francesca Ronchi[2], Katrien van der Borght[3], Rebekka Niederer[1], Lucas Onder[1], Mechthild Lütge[1], Mario Novkovic[1], Veronika Nindl[1], Gustavo Ramos[4,5], Markus Arnoldini[6], Emma M.C. Slack[6], Valérie Boivin-Jahns[5,7], Roland Jahns[5,8], Madeleine Wyss[9], Catherine Mooser[2], Bart N. Lambrecht[3], Micha T. Maeder[10], Hans Rickli[10], Lukas Flatz[1], Urs Eriksson[11,12], Markus B. Geuking[13], Kathy D. McCoy[9], Burkhard Ludewig[1]*

Myocarditis can develop into inflammatory cardiomyopathy through chronic stimulation of myosin heavy chain 6–specific T helper (T_H)1 and T_H17 cells. However, mechanisms governing the cardiotoxicity programming of heart-specific T cells have remained elusive. Using a mouse model of spontaneous autoimmune myocarditis, we show that progression of myocarditis to lethal heart disease depends on cardiac myosin–specific T_H17 cells imprinted in the intestine by a commensal *Bacteroides* species peptide mimic. Both the successful prevention of lethal disease in mice by antibiotic therapy and the significantly elevated *Bacteroides*-specific $CD4^+$ T cell and B cell responses observed in human myocarditis patients suggest that mimic peptides from commensal bacteria can promote inflammatory cardiomyopathy in genetically susceptible individuals. The ability to restrain cardiotoxic T cells through manipulation of the microbiome thereby transforms inflammatory cardiomyopathy into a targetable disease.

Myocarditis is an inflammatory heart disease that can develop into lethal cardiomyopathy (*1*–*3*). Acute immune activation during myocarditis is associated with the generation of autoimmune responses against myosin heavy chain 6 (MYH6) (*4*–*7*). Subsequent chronic stimulation of MYH6-specific T helper (T_H)1 and T_H17 cells precipitates inflammatory cardiomyopathy (*8*–*11*). The progressive nature of autoimmune and chronic inflammatory diseases is determined by genetic susceptibility and distinct environmental conditions (*12*, *13*). Susceptibility to inflammatory cardiomyopathy can be associated with HLA-DQB1* polymorphisms (*14*, *15*), whereas infection with pathogens predisposes patients, due to the death of cardiomyocytes and excessive presentation of self-antigens, to major histocompatibility complex (MHC) class II–restricted T cells (*16*). Alternatively, the antigenic mimicry of microbial components may drive these diseases (*16*–*19*).

To assess whether heart-specific T cells cross-react with microbial components, we used transgenic mice expressing a MYH6-specific T cell receptor on more than 95% of their $CD4^+$ T cells (TCRM) (*10*). All TCRM mice developed spontaneous autoimmune myocarditis, and ~50% of the animals progressed to lethal cardiomyopathy under specific pathogen–free (SPF) housing conditions (Fig. 1, A to D). In contrast, the lack of a commensal microbiome under germ-free (GF) conditions blunted the lethal disease outcome (Fig. 1A), abrogated cardiac dilatation (Fig. 1B), substantially reduced cardiac fibrosis (Fig. 1C), and significantly reduced disease severity (Fig. 1D). Echocardiographic analysis revealed that the hearts of GF TCRM mice functioned normally despite low-level cardiac inflammation (Fig. 1, E to G). Recolonization of GF TCRM mice with the SPF microbiome (fig. S1A) precipitated progression to lethal disease in ex-GF mice within 6 to 12 weeks (Fig. 1H), significantly exacerbated cardiac inflammation (Fig. 1I), and impaired cardiac function (fig. S1, B to D). Moreover, microbial colonization of GF TCRM mice exacerbated cardiac immune cell infiltration (Fig. 1J), including transgenic MYH6-specific $CD4^+$ T cells (Fig. 1K). The activity of heart-infiltrating TCRM T_H17 cells (Fig. 1L), but not T_H1 cells (Fig. 1M), depended on the microbial status of the mouse. Cohousing increased the fraction of both T_H1 (Fig. 1M) and T_H17 heart-specific $CD4^+$ T cells (Fig. 1L) and promoted the accumulation of inflammatory myeloid cells in the heart tissue (Fig. 1, N to Q, and fig. S1, E to H), including inflammatory monocytes (Fig. 1O), activated macrophages (Fig. 1P), and resident macrophages (Fig. 1Q). Thus, the presence of the microbiota fosters the imprinting of a T_H17 phenotype in heart-specific $CD4^+$ T cells and favors the accumulation of myeloid cells in the myocardia of TCRM mice.

Heart-infiltrating $CD4^+$ TCRM cells showed significantly elevated expression of gut-homing receptors under SPF compared with GF conditions (Fig. 2A), and they homed to the T cell zones of colonic patches (Fig. 2B), colonic lymph nodes, and mesenteric lymph nodes in an adoptive transfer–model (fig. S2, A to C). Transferred TCRM T cells proliferated initially in the lamina propria, the colonic lymph node, and the mediastinal lymph node, and they subsequently migrated to the heart tissue (Fig. 2C and fig. S2D). Th cell responses in the hearts of TCRM mice were dominated by T_H1 cells (fig. S2E), whereas the colonic lamina propria environment fostered the differentiation of T_H17 cells (fig. S2, E and F). Next-generation sequencing of fecal 16*S* ribosomal RNA (rRNA) genes revealed that cohoused transgene-negative (Tg^-) and TCRM mice possessed disparate microbiomes (fig. S2G). Cohousing with GF TCRM mice (fig. S2H) showed that the microbiome of ex-GF TCRM mice was more similar to the SPF TCRM microbiome than the SPF wild-type microbiome (Fig. 2D) and suggested that GF TCRM mice acquired the microbiome of SPF TCRM mice (Fig. 2E and fig. S2I). An in silico search revealed two potentially cross-reactive β-galactosidase (β-gal) mimic peptides in *Bacteroides thetaiotaomicron* (*B. theta*) and *B. faecis* with high similarity to MYH6 (table S1). $CD4^+$ TCRM T cells exhibited a functional avidity of 6.3×10^{-6} M for the *B. theta* peptide (fig. S3A), facilitating the efficient activation of TCRM T cells in vitro and in vivo (Fig. 2, F to H). Monocolonization of GF TCRM mice with *B. theta* or *Escherichia coli* (*E. coli*), or with our SPF microbiota (fig. S3C), showed that *B. theta* monocolonization fostered mainly the induction of T_H17 cells (fig. S3D). Monocolonization of GF TCRM mice with a *B. theta* mutant lacking the β-gal *BT1626* gene encoding for the MYH6 peptide mimic (*B. theta* Δβgal) (fig. S3, E and F) or the parental strain resulted in the efficient seeding of the gut with both strains (fig. S3G). However, recolonization of TCRM mice with *B. theta* Δβgal reduced the accumulation of immune cells in the myocardium (Fig. 2I) and significantly diminished the activity of myosin-specific T_H17 cells in the heart and colon (Fig. 2J). Moreover, the presence of TCRM cells substantially increased the production of immunoglobulin A (IgA) against commensal microbiota under SPF conditions (fig. S3, H and I), whereas the absence of the cross-reactive epitope in *B. theta* Δβgal led to a significantly reduced IgA response in

[1]Institute of Immunobiology, Kantonsspital St. Gallen, St. Gallen, Switzerland. [2]Maurice Müller Laboratories, Department of Biomedical Research, Universitätsklinik für Viszerale Chirurgie und Medizin Inselspital, University of Berne, Berne, Switzerland. [3]VIB Center for Inflammation Research, Department of Internal Medicine and Pediatrics, Ghent University, Ghent, Belgium. [4]Department of Internal Medicine I, University Hospital Würzburg, Würzburg, Germany. [5]Comprehensive Heart Failure Center, University Hospital of Würzburg, Würzburg, Germany. [6]Institute of Food, Nutrition and Health, ETH, Zurich, Switzerland. [7]Institute of Pharmacology and Toxicology, University of Würzburg, Würzburg, Germany. [8]Interdisciplinary Bank of Biomaterials and Data Würzburg (IBDW), University Hospital of Würzburg, Würzburg, Germany. [9]Department of Physiology and Pharmacology, Snyder Institute for Chronic Diseases, Cumming School of Medicine, University of Calgary, Calgary, AB, Canada. [10]Cardiology Division, Kantonsspital St. Gallen, St. Gallen, Switzerland. [11]Center for Molecular Cardiology University of Zurich, Zurich, Switzerland. [12]Department of Medicine, GZO Regional Health Center, Wetzikon, Switzerland. [13]Department of Microbiology, Immunology and Infectious Diseases, Snyder Institute for Chronic Diseases, Cumming School of Medicine, University of Calgary, Calgary, AB, Canada.
*Corresponding author. Email: burkhard.ludewig@kssg.ch

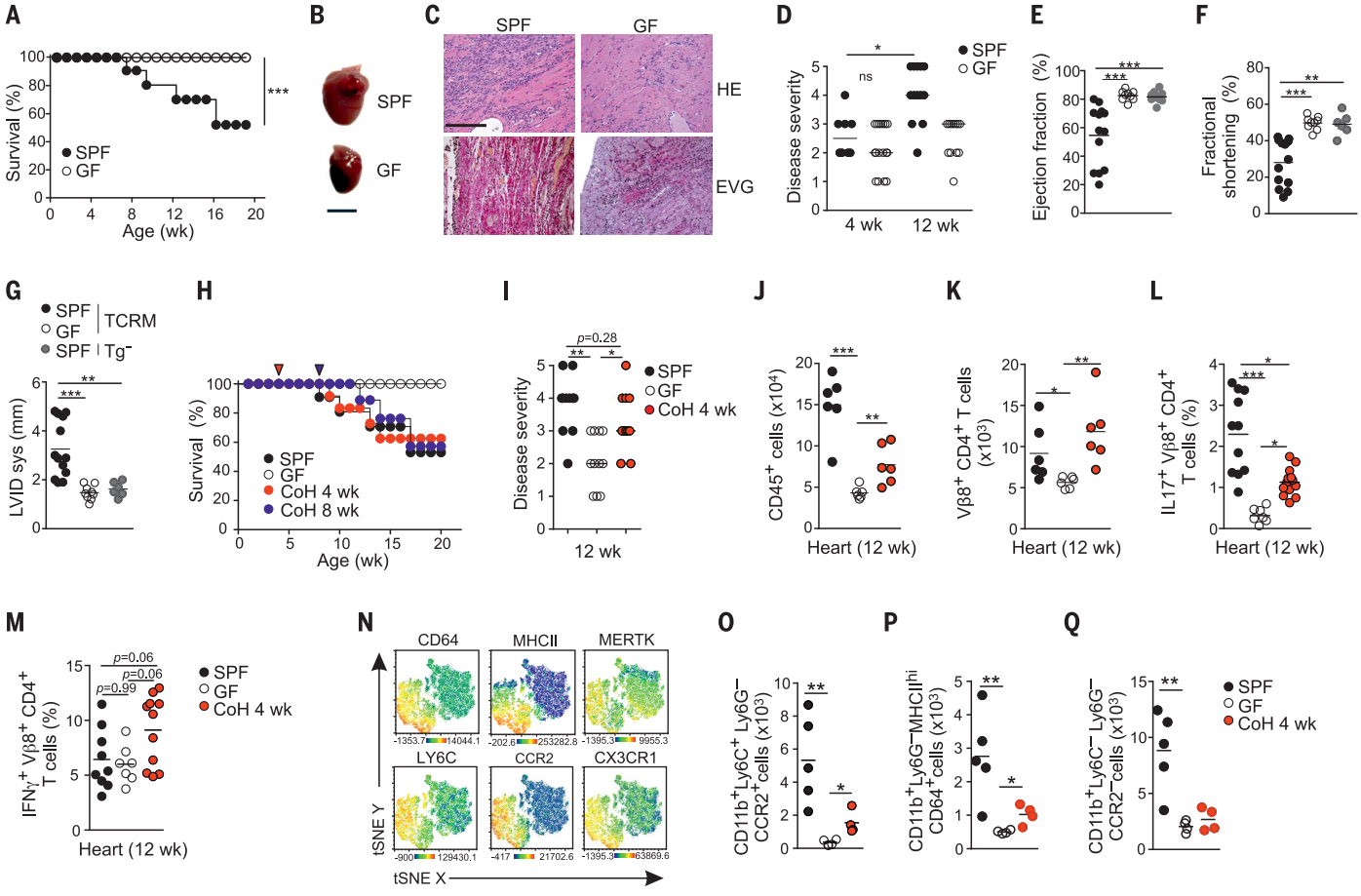

Fig. 1. Microbiome-dependent transition of autoimmune myocarditis to dilated cardiomyopathy. (**A**) Survival of TCRM mice under SPF or GF conditions. wk, weeks. (**B**) Gross pathology of hearts from 12-week-old SPF TCRM and age-matched GF TCRM mice. Scale bar, 4 mm. (**C**) Histological analysis of hearts of 12-week-old TCRM mice kept under SPF or GF conditions, using hematoxylin-eosin (HE) and Elastica–van Gieson (EVG) staining. Scale bar, 100 μm. (**D**) Histopathological disease severity in TCRM mice under SPF and GF conditions, determined at the indicated ages. Dots represent values of individual mice and lines indicate median values. ns, not significant. (**E** to **G**) Echocardiographic parameters in SPF or GF TCRM mice and in transgene-negative littermates of controls (Tg^-) with (E) ejection fraction, (F) fractional shortening, and (G) systolic left ventricular internal diameter (LVID sys) determined in individual mice. (**H** to **Q**) GF TCRM mice were transferred to SPF conditions and cohoused with SPF TCRM mice from 4 (CoH 4 wk) or 8 (CoH 8 wk) weeks of age until analysis. For comparison, TCRM mice under GF or SPF conditions were used. (H) Prospective survival analysis. Arrowheads indicate the age of transfer to SPF conditions. (I) Histopathological disease progression. Dots represent individual mice and lines indicate median values. Enumeration of heart-infiltrating cells: (J) $CD45^+$ cells and (K) myosin-specific $CD4^+$ T cells ($Vβ8^+CD4^+$); (L) IL-17– (interleukin-17–) and (M) IFN-γ–producing heart-infiltrating MYH6-specific $CD4^+$ T cells ($Vβ8^+CD4^+$). (N to Q) Heart-infiltrating myeloid cell subsets analyzed by flow cytometry. (N) Representative t-distributed stochastic neighbor embedding (t-SNE) plots of $CD11b^+Ly6G^-$ cells in the hearts of SPF TCRM mice. Enumeration of (O) inflammatory monocytes, (P) $MHCII^{hi}$ macrophages, and (Q) $CD11b^-CCR2^-$ cardiac-resident macrophages. Dots represent individual mice and lines indicate mean values. Pooled data from two independent experiments with n = 4 to 7 mice [(J), (K), (O) to (Q)] or three independent experiments with ≥15 mice [(A) and (H)], ≥12 mice [(B), (C), and (D)], ≥6 mice [(E) to (G)], or ≥7 mice [(L) and (M)] per group. Representative micrographs from one out of at least 12 mice [(B) and (C)]. Statistical analysis was performed using Mantel-Cox test (A) or Kruskall-Wallis H test [(D) and (I)] or one-way analysis of variance (ANOVA) with Dunnett's multiple comparison test [(E) to (G), (J) to (N), and (O) to (Q)] with $*P < 0.05$; $**P < 0.01$; $***P < 0.001$.

monocolonized TCRM mice (Fig. 2, K and L). Thus, heart-specific $CD4^+$ T cells can shape the colonic microbiome, and distinct bacterial communities—in this case, *Bacteroides*—provide mimic peptides that can activate MYH6-specific $CD4^+$ T cells.

Modification of the microbiome by antibiotic treatment (fig. S4A) prevented lethal cardiomyopathy (Fig. 3A) and reduced cardiac inflammation (Fig. 3B). Adoptive transfer of TCRM splenocytes into antibiotics-treated $Rag1^{-/-}$ mice (fig. S4B) revealed that broad-spectrum antibiotics not only reduced *B. theta* levels in fecal samples (Fig. 3C) but significantly ameliorated cardiac disease at day 28 after adoptive transfer (Fig. 3D). There was a significantly reduced accumulation of $CD45^+$ immune cells (Fig. 3E) and TCR-transgenic $CD4^+$ T cells (Fig. 3F) in the hearts of $Rag1^{-/-}$ recipients treated with various antibiotics. Broad-spectrum antibiotic regimens primarily reduced immune cell accumulation in the colons (fig. S4, C and D), but not in the spleens (fig. S4E), and had a pronounced impact on the cytokine production by heart-infiltrating and colonic T_H17 cells. T_H1 cell activity was also reduced, but to a lesser extent (Fig. 3G and fig. S4, F and G). Antibiotic treatment reduced *B. theta*–specific IgG antibody levels, but the treatment had variable effects on IgG antibody responses against *B. distasonis*, *B. vulgatus*, or *E. cloacae* (Fig. 3H). Moreover, the adoptive transfer of heart-specific TCRM cells to BALB/c mice

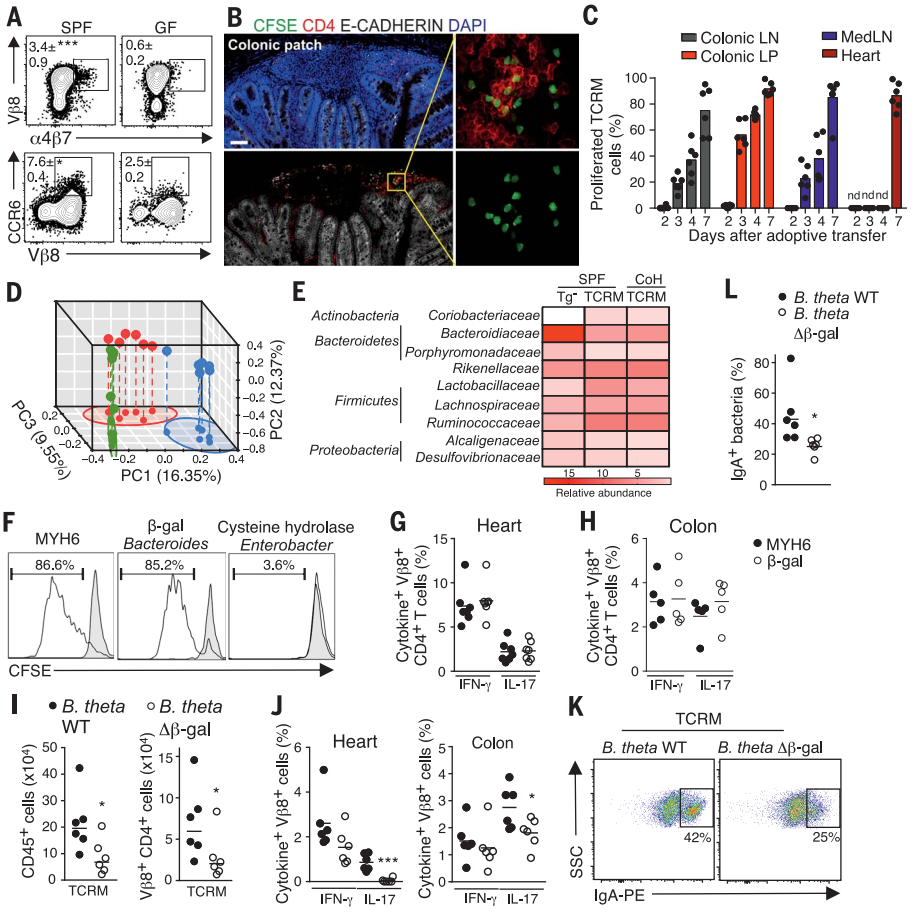

Fig. 2. Interaction of MYH6-specific CD4$^+$ T cells with the intestinal microbiome. (**A**) Flow cytometric analysis of α4β7-integrin and CCR6 in heart-infiltrating MYH6-specific cells from SPF or GF TCRM mice. (**B** and **C**) Location and proliferation of carboxyfluorescein succinimidyl ester (CFSE)–labeled TCRM cells after adoptive transfer to *Rag1*$^{-/-}$ mice. (B) Confocal microscopy analysis of colonic patches at day 3 after adoptive transfer. Scale bar, 100 μm. DAPI, 4′,6-diamidino-2-phenylindole. (C) Proliferation of MYH6-specific cells. CFSE dilution in the indicated organs and at the indicated time points is quantified by flow cytometry. Bars indicate mean values. nd, not detectable; LN, lymph node; LP, lamina propria; MedLN, mediastinal lymph node. (**D** and **E**) Fecal bacterial composition of transgene-negative littermate controls (Tg$^-$), SPF TCRM, and GF TCRM mice cohoused at 4 weeks of age under SPF conditions by 16*S* rRNA sequencing. (D) Principal component (PC) analysis. (E) Heat map of the relative abundance of the indicated bacterial classes and families. (**F** to **H**) MYH6-specific CD4$^+$ T cell cross-reactivity. (F) In vitro proliferation of CD4$^+$ T cells from TCRM mice after restimulation with MYH6, β-gal peptide from *Bacteroides*, or cysteine hydrolase-derived peptide from *E. cloacae* determined by CFSE-dilution assay. (G and H) Cytokine production of heart- and colon-infiltrating, Vβ8-expressing CD4$^+$ T cells from SPF TCRM mice after ex vivo restimulation with MYH6 or *Bacteroides* β-gal peptides. Dots represent values from individual mice, lines indicate mean values. (**I** to **L**) GF TCRM mice were monocolonized with *B. theta* wild type (*B. theta* WT) or *B. theta* lacking the β-galactosidase *BT1626* gene (*B. theta* Δβ-gal). (I and J) Flow cytometric analysis of (I) heart-infiltrating cells and (J) MYH6-specific cytokine producing cells in the heart and colon. Dots represent values from individual mice and lines indicate mean values. (K and L) IgA-bound fecal bacteria determined by bacterial flow cytometry (K) and pooled data from individual mice. Lines indicate mean values (L). SSC, side scatter; PE, phycoerythrin. Pooled data from $n = 6$ [(A) to (E), (J) to (L)], $n = 7$ (G), and $n = 5$ (H) mice from at least two independent experiments. Representative plots showing percentage ± SEM (A). Representative histograms from two independent experiments with duplicates (F). Representative plots and percentage values of IgA-bound bacteria are indicated (K). Statistical analysis was performed using Student's *t* test [(A), (G), (H), (I), (J), and (L)] or one-way ANOVA with Tukey's multiple comparison test (E) with $^*P < 0.05$; $^{***}P < 0.001$.

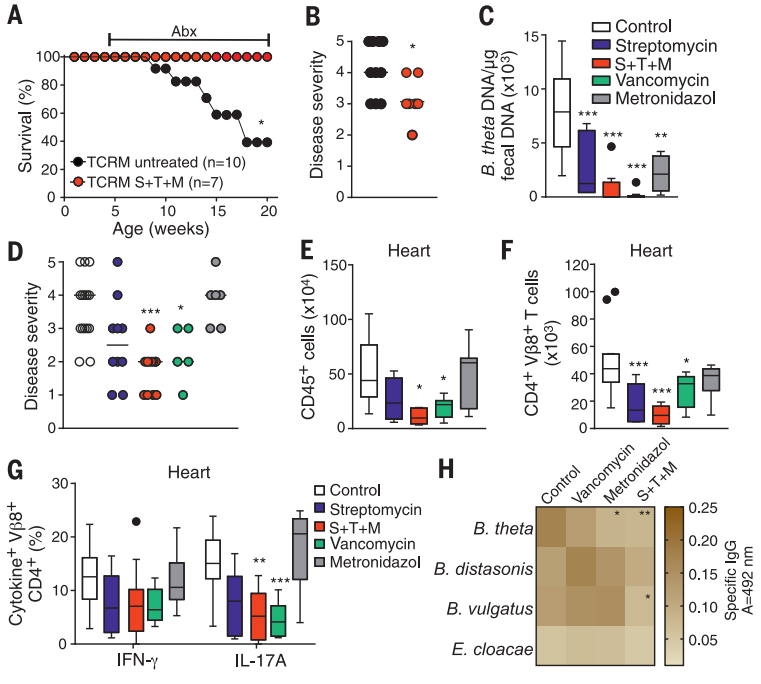

Fig. 3. Impact of antibiotic treatment on lethal heart disease and immune reactivity in the TCRM model. (**A**) Survival of and (**B**) disease severity in TCRM mice after postweaning treatment with a broad-spectrum antibiotics combination comprising sulphadoxine, trimethoprim, and metronidazole (S+T+M). Disease severity was determined in 20-week-old mice. Dots represent values of individual mice and bar indicates mean disease severity. Abx, S+T+M. (**C** to **H**) *Rag1*$^{-/-}$ mice were adoptively transferred with 10^6 TCRM splenocytes to induce fast progressing myocarditis; mice were treated or left untreated with the indicated oral antibiotics until analysis (day 28 after adoptive transfer). (C) *B. theta* quantification in feces by quantitative polymerase chain reaction. (D) Histopathological analysis of hearts. Dots represent values of individual mice and lines indicate median disease severities. (E and F) Quantification of heart-infiltrating CD45$^+$ cells (E) and Vβ8-expressing CD4$^+$ T cells (F). (G) Cytokine production of heart-infiltrating MYH6-specific Vβ8$^+$CD4$^+$ T cells. (C and E to G) Box-and-whisker plots show mean values ± the interquartile range; black dots indicate outliers. (H) Heat map of the specific IgG responses against *B. theta, B distasonis, B. vulgatus*, and *E. cloacae* determined by enzyme-linked immunosorbent assay (ELISA). Pooled data from two to three independent experiments with $n = 7$ to 10 [(A) and (B)] and $n = 5$ to 13 [(C) to (H)]. Statistical analysis was performed using the Mann-Whitney *U* test (B); or one-way ANOVA with Dunnett's multiple comparison test [(C), (E) to (H)] or Kruskall-Wallis *H* test (D) with $^*P < 0.05$; $^{**}P < 0.01$; $^{***}P < 0.001$.

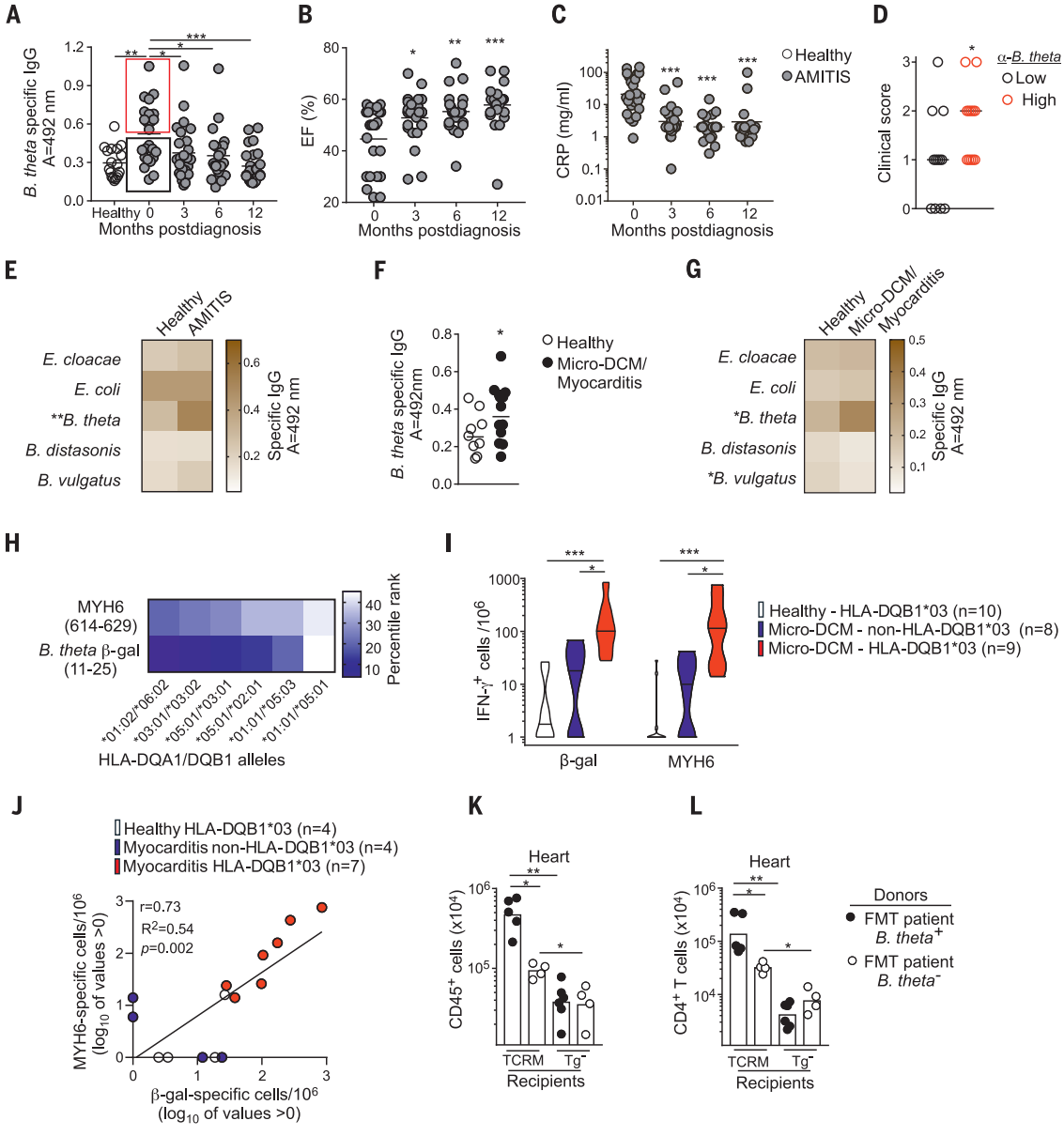

Fig. 4. Immune reactivity against *Bacteroides* and cardiac myosin antigens in human myocarditis patients. (**A**) Analysis of *B. theta*–specific IgG antibodies in sera of myocarditis patients from the AMITIS cohort at admission and different time points post-diagnosis compared with sera from healthy individuals. Red and black boxes indicate patients with high or low anti–*B. theta* antibody levels, respectively. Dots represent individual antibody levels and lines indicate mean values. A, absorbance. (**B**) Ejection fraction (EF) and (**C**) C-reactive protein (CRP) values in patients from the AMITIS cohort at the indicated time points. Dots represent individual values and lines indicate mean values. (**D**) Composite clinical scores of myocarditis patients from the AMITIS cohort with low versus high IgG antibodies against *B. theta* at their first visit [as indicated in (A)]. Dots represent individual clinical scores as the sum of positivity for anti-beta1-AR antibodies, CRP values ≥16 and EF ≤40, and lines indicate median clinical scores. (**E**) Heat map of specific IgG response against *B. theta*, *B. distasonis*, *B. vulgatus*, and *E. cloacae* in the AMITIS cohort and healthy controls. (**F**) Serum *B. theta*–specific IgG levels in patients from the Micro-DCM cohort at admission. Dots represent individual patient values and lines indicates mean values. (**G**) Heat map of antibacterial IgG reactivity. (**H**) Heat map representing the in silico predicted binding of the $MYH6_{614-629}$ peptide or the *B. theta* β-gal_{11-25} peptide to prevalent HLA-DQ alleles. (**I**) IFN-γ enzyme-linked immunospot (ELISPOT) analysis of peripheral blood mononuclear cells of HLA-DQB1*03 healthy volunteers (n = 10) or Micro-DCM cohort patients (HLA-DQB1*03 n = 9; other HLA n = 8) after stimulation with the human $MYH6_{614-629}$ peptide or the *B. theta* β-gal_{11-25} peptides. Violin plots show mean values ± interquartile ranges. (**J**) Correlation between MYH6- or β-gal IFN-γ–producing cells in myocarditis patients and healthy individuals with the indicated HLA-DQB1 alleles. Dots represent individual subjects. r, Pearson correlation coefficient; R^2, coefficient of determination. (**K** and **L**) Enumeration of heart-infiltrating $CD45^+$ immune cells (K) and $CD4^+$ T cells (L) in ex-GF recipient mice 4 weeks after fecal microbiome transplantation (FMT). Dots represent values of individual mice and bars indicate mean values. Statistical analysis was performed using one-way ANOVA with Dunnett's multiple comparison test [(A) to (C) and (I)] or Mann-Whitney U test (D) or Student's t test [(E) to (G)] and [(K) and (L)] or the Pearson correlation coefficient with two-tailed P-value calculation (J) with *P < 0.05; **P < 0.01; ***P < 0.001.

significantly enhanced anti–*B. theta* antibody responses (fig. S4H). Therefore, heart-specific $CD4^+$ T cells specifically interact with microbial components in the intestine, thereby affecting systemic immune reactivity.

To establish translational relevance of these findings, we assessed serum anti-*Bacteroides* IgG responses from human patients with biopsy-confirmed acute myocarditis (table S2) (*20*). These patients showed significantly elevated *B. theta*–specific IgG responses when compared with a healthy control group (Fig. 4A). Clinical improvement of these myocarditis patients (Fig. 4, B and C) was accompanied by a reduction in seroreactivity against *B. theta* (Fig. 4A). Patients with low anti–*B. theta* IgG reactivity (black box in Fig. 4A) showed a combined clinical score (fig. S5, A to C) that was significantly lower than that of the high-responder group (Fig. 4D). Although IgG antibodies against *B. theta* in myocarditis patients were diminished during subsequent visits (Fig. 4A), anti-*E. cloacae* antibodies (fig. S5D), anti-*E. coli* antibodies (fig. S5E), and total serum IgG levels (fig. S5F) did not change significantly. Moreover, IgG antibody reactivity against other *Bacteroides* species did not differ between

myocarditis patients and healthy controls (Fig. 4E). Likewise, myocarditis patients recruited in a prospective clinical study (table S3) showed significantly elevated anti–*B. theta* IgG antibodies (Fig. 4, F and G) when compared with healthy volunteers (table S4). Bioinformatics analysis of binding affinities of the *B. theta* β-gal$_{11\text{-}25}$ peptide mimic indicated several HLA-DQA1*/B1* combinations that are also predicted to bind human MYH6$_{614\text{-}629}$ (Fig. 4H). Peripheral blood T cells from patients exhibited significantly higher interferon-γ (IFN-γ) reactivity against the MYH6 and β-gal peptides when compared with healthy controls (Fig. 4I). Moreover, there was a highly significant correlation between MYH6 and β-gal$_{11\text{-}25}$ peptide reactivity (Fig. 4J), indicating that heart-specific CD4$^+$ T cells cross-react with the bacterial peptide in human myocarditis patients. Finally, GF TCRM and Tg$^-$ mice (fig. S5, K and L) received fecal transplants from myocarditis patients positive or negative for *B. theta*. The accumulation of immune cells (Fig. 4, K and L) was significantly increased only in the hearts of TCRM mouse recipients given transplants from patients positive for *B. theta*. Thus, it is conceivable that inflammatory cardiomyopathy in humans is driven, at least in part, through the activation of heart-specific Th cells by bacterial peptide mimics derived from the intestinal microbiota.

Overall, in this scenario, cross-reactive CD4$^+$ T cells primed in the intestine can enter the myocardium and exacerbate the damage caused by infection by cardiotropic viruses or subclinical myocardial infarction (fig. S5M). Likewise, the loss of control over self- and cross-reactive T cells during immune checkpoint inhibitor therapy may be a reason for potentially lethal cardiac inflammation in patients who share particular *HLADQA1*/B1** alleles (*21*–*23*). Thus, targeting the microbiome of genetically predisposed myocarditis patients or susceptible patients undergoing checkpoint inhibitor treatment through antibiotics may alleviate disease severity and may therefore help prevent the potentially lethal sequelae of inflammatory cardiomyopathy.

REFERENCES AND NOTES

1. J. Buggey, C. A. ElAmm, *Curr. Opin. Cardiol.* **33**, 341–346 (2018).
2. R. G. Weintraub, C. Semsarian, P. Macdonald, *Lancet* **390**, 400–414 (2017).
3. L. T. Cooper Jr., A. Keren, K. Sliwa, A. Matsumori, G. A. Mensah, *Glob. Heart* **9**, 121–129 (2014).
4. N. R. Rose, *F1000Prime Rep.* **6**, 25 (2014).
5. B. H. Trachtenberg, J. M. Hare, *Circ. Res.* **121**, 803–818 (2017).
6. P. Krebs *et al*., *J. Autoimmun.* **28**, 224–233 (2007).
7. N. Neu *et al*., *J. Immunol.* **139**, 3630–3636 (1987).
8. M. Rangachari *et al*., *J. Exp. Med.* **203**, 2009–2019 (2006).
9. H. Lv *et al*., *J. Clin. Invest.* **121**, 1561–1573 (2011).
10. V. Nindl *et al*., *Eur. J. Immunol.* **42**, 2311–2321 (2012).
11. J. M. Myers *et al*., *JCI Insight* **1**, e85851 (2016).
12. E. Generali, A. Ceribelli, M. A. Stazi, C. Selmi, *J. Autoimmun.* **83**, 51–61 (2017).
13. A. Davidson, B. Diamond, *N. Engl. J. Med.* **345**, 340–350 (2001).
14. W. Liu, W. M. Li, N. L. Sun, *Ann. Hum. Genet.* **69**, 382–388 (2005).
15. I. Portig, A. Sandmoeller, S. Kreilinger, B. Maisch, *Autoimmunity* **42**, 33–40 (2009).
16. S. Heymans, U. Eriksson, J. Lehtonen, L. T. Cooper Jr., *J. Am. Coll. Cardiol.* **68**, 2348–2364 (2016).
17. B. Maisch, P. Alter, *Herz* **43**, 423–430 (2018).
18. C. Massilamany, S. A. Huber, M. W. Cunningham, J. Reddy, *J. Cardiovasc. Transl. Res.* **7**, 165–171 (2014).
19. N. Tai *et al*., *J. Exp. Med.* **213**, 2129–2146 (2016).
20. N. Deubner *et al*., *Eur. J. Heart Fail.* **12**, 753–762 (2010).
21. D. B. Johnson *et al*., *N. Engl. J. Med.* **375**, 1749–1755 (2016).
22. L. Zhang *et al*., *Curr. Treat. Options Cardiovasc. Med.* **21**, 32 (2019).
23. Y. Zamami *et al*., *JAMA Oncol.* 10.1001/jamaoncol.2019.3113 (2019).
24. C. Gil-Cruz *et al*., Microbiota-derived peptide mimics drive lethal inflammatory cardiomyopathy. Figshare (2019); https://figshare.com/s/229fc19d6d8db36ad1db

ACKNOWLEDGMENTS

We thank S. Caviezel-Firner, C. Engetschwiler, and R. De Guili for technical support. **Funding:** This study received financial support from the Swiss National Science Foundation (grants 130823 and 146133 to B.L.); the Interdisciplinary Centre for Clinical Research (IZKF Würzburg), Grant IZKF, project E-32; and the Bundesministerium für Bildung und Forschung (BMBF), grant "Molecular Diagnostics" FKZ 01ES0901 and FKZ 01ES0802 (to V.B.-J. and R.J.). G.R. received support from the Interdisciplinary Centre for Clinical Research (E-354). L.F. is supported by a Swiss National Science Foundation professorship (PP00P3_157448). The funders had no role in study design, data collection and analysis, decision to publish, or preparation of the manuscript. **Author contributions:** B.L. designed the study, discussed data, and wrote the paper; C.G.-C. and C.P.-S. designed the study, performed experiments, and wrote the paper; A.D.M., K.v.d.B., V.N., F.R., R.N., L.O., M.L., M.N., M.A., M.W., and C.M. performed experiments and discussed data; G.R., E.M.C.S., V.B.-J., R.J., B.N.L., U.E., M.B.G., H.R., L.F., and K.D.M. discussed data and provided reagents; B.L. and M.T.M. designed the Micro-DCM cohort and account responsible for this study. **Competing interests:** The authors declare no competing interests. **Data and materials availability:** All sequence data are accessible at Figshare (*24*). All other data needed to evaluate the conclusions in the paper are available within the main text or supplementary materials. The TCRM mouse strain is available under a materials transfer agreement from the authors.

SUPPLEMENTARY MATERIALS

science.sciencemag.org/content/366/6467/881/suppl/DC1
Materials and Methods
Figs. S1 to S5
Tables S1 to S6
References (*25*–*36*)

View/request a protocol for this paper from *Bio-protocol*.

7 September 2018; resubmitted 13 June 2019
Accepted 9 October 2019
10.1126/science.aav3487

Science

Microbiota-derived peptide mimics drive lethal inflammatory cardiomyopathy

Cristina Gil-Cruz, Christian Perez-Shibayama, Angelina De Martin, Francesca Ronchi, Katrien van der Borght, Rebekka Niederer, Lucas Onder, Mechthild Lütge, Mario Novkovic, Veronika Nindl, Gustavo Ramos, Markus Arnoldini, Emma M.C. Slack, Valérie Boivin-Jahns, Roland Jahns, Madeleine Wyss, Catherine Mooser, Bart N. Lambrecht, Micha T. Maeder, Hans Rickli, Lukas Flatz, Urs Eriksson, Markus B. Geuking, Kathy D. McCoy and Burkhard Ludewig

Science **366** (6467), 881-886.
DOI: 10.1126/science.aav3487

Peptide mimicry breaks the heart

Myocarditis, a prolonged chronic inflammation of heart muscle, can eventually progress to inflammatory cardiomyopathy, a serious condition associated with heart failure. Activated T helper (T_H) cells that recognize myosin heavy chain 6–derived peptides are thought to play a central role in this pathogenesis. Using a mouse model of myocarditis, Gil-Cruz *et al.* found that cardiac myosin–reactive T_H cells are initially primed by myosin-peptide mimics derived from commensal *Bacteroides* species in the gut (see the Perspective by Epelman). Unlike heathy controls, human myocarditis patients also showed detectable immune reactivity to both *Bacteroides* and cardiac myosin antigens. Treatment with antibiotics dampened inflammatory responses and prevented lethal heart disease.

Science, this issue p. 881; see also p. 806

Science (print ISSN 0036-8075; online ISSN 1095-9203) is published by the American Association for the Advancement of Science, 1200 New York Avenue NW, Washington, DC 20005. The title *Science* is a registered trademark of AAAS.